

# Ferroelectric domains in nitrobenzene-nitromethane solutions measured by hyper-Rayleigh scattering

David P. Shelton<sup>a)</sup>*Department of Physics, University of Nevada Las Vegas, Las Vegas, Nevada 89154-4002*

(Received 3 January 2006; accepted 9 February 2006; published online 27 March 2006)

Hyper-Rayleigh scattering (HRS) spectra were measured for liquid solutions of  $C_6H_5NO_2$  and  $CH_3NO_2$  at  $T=300$  K. The depolarized HRS spectra at small frequency shift are dominated by two components due to reorientation of the nitrobenzene molecules. One is a Lorentzian with spectral width  $\nu_1=0.16-0.45$   $cm^{-1}$  and corresponding orientation relaxation time  $\tau=33-12$  ps. The second component is a narrow spike with spectral width  $<2$  MHz and corresponding relaxation time  $\tau > 80$  ns, attributed to HRS from slowly relaxing ferroelectric domains. The dipole order parameter  $g_0=0.053\pm 0.005$ , saturation parameter  $p=0.9\pm 0.1$ , and volume  $V=20\pm 6$   $nm^3$  for these domains in nitromethane were determined from measurements of the nitrobenzene-concentration dependence of the intensity ratio for these two spectral components. Orientation of the 230 nitromethane molecules within each domain is inhomogeneous but highly ordered. © 2006 American Institute of Physics. [DOI: 10.1063/1.2181980]

## I. INTRODUCTION

Recent hyper-Rayleigh scattering (HRS) experiments studying liquid water,<sup>1,2</sup> acetonitrile,<sup>3,4</sup> and nitromethane<sup>5</sup> find a narrow peak in the depolarized HRS spectrum, with spectral width  $<5$  MHz and corresponding relaxation time  $>30$  ns, and attribute this peak to ferroelectric domains in the liquid.<sup>3</sup> These experiments measure the second-harmonic light scattered at  $90^\circ$  by the liquid sample, with the incident laser beam linearly polarized perpendicular ( $V$ ) or parallel ( $H$ ) to the horizontal scattering plane and with  $V$  or  $H$  linear polarization selected for the scattered light, allowing polarized ( $VV$  incident and scattered polarization) or depolarized ( $HV$ ,  $VH$ ,  $HH$ ) HRS to be observed. The narrow peak seen in the  $VH$  HRS spectrum is absent from the  $VV$  and  $HV$  spectra, which shows that it is due to a longitudinal polar collective mode of the molecules.<sup>3,6-8</sup> Long-lived polar order for the molecules may occur by the formation of ferroelectric domains when the number density  $\rho$  of molecules with dipole moment  $\mu$  exceeds the threshold value  $\rho\mu^2=9\epsilon_0k_B T=49$   $D^2$  M at  $T=300$  K.<sup>3</sup> The idea of ferroelectric domains in dipolar liquids is supported by a HRS experiment in which the narrow  $VH$  peak is observed to disappear when  $\rho\mu^2$  for acetonitrile is reduced to the predicted ferroelectric threshold by dilution of the acetonitrile with a nonpolar liquid.<sup>3</sup>

Ferroelectric fluid phases are found in model calculations where the molecules are composed of a point dipole at the center of a hard sphere or ellipsoid<sup>9</sup> or a soft sphere.<sup>10,11</sup> The orientational order for the dipoles in the ferroelectric domain obtained from such a model calculation for the Stockmayer liquid has the form of a planar vortex which “escapes” along the axis.<sup>10,11</sup> This model differs from a real bulk liquid in that the only anisotropy of the molecular interaction potential is due to the dipole interaction, and also

because the simulated volume contains only about 400 molecules. Nevertheless, domains with the polarization vortex spatial structure suggested by this model have a small depolarizing field and can fill space, and so may also appear in real dipolar liquids. Similar structures are found in simulations of solid ferroelectric nanoparticles.<sup>12,13</sup> An example of macroscopic polar order observed in a real liquid is the incommensurate helical polarization with micrometer pitch observed in chiral tilted smectic ferroelectric liquid crystals,<sup>14</sup> although the order in this liquid crystal arises primarily from short range steric interactions between the molecules. While the spatial pattern and the length scale of the polar molecular order are very different in these two liquid examples, reduction of depolarizing fields favors spatially inhomogeneous polarization in both.

The goal of the present work is to characterize the degree of order and the size of the ferroelectric domains revealed by previous HRS experiments. This is accomplished using nitrobenzene molecules to probe the domains in nitrobenzene-nitromethane solutions. Nitrobenzene is chosen as the probe since it gives a strong HRS signal and the molecules have size and dipole moment similar to nitromethane.

## II. THEORETICAL MODEL

Consider a liquid composed of dipolar molecules with number density  $\rho$ , partitioned into small domains of volume  $V$ . Each domain contains  $M=\rho V$  molecules, and the average number of oriented molecules in a domain is  $\langle N \rangle = gM$ . Since the domains are small compared to the wavelength of light, the light scattered from the oriented molecules in a domain adds coherently, with intensity  $\propto \langle N^2 \rangle = \langle N \rangle + \langle N \rangle^2$ . The other  $M - \langle N \rangle = (1-g)M$  molecules in a domain are randomly oriented, so the scattering from these molecules adds incoherently with intensity  $\propto (1-g)M$ . Finally, scattering from adjacent randomly oriented domains adds incoherently. The ratio

<sup>a)</sup>Electronic mail: shelton@physics.unlv.edu

$R$  of coherent and incoherent HRS intensities expressed as a function of the domain order parameter  $g$  and volume  $V$  is

$$R = [\langle N \rangle + \langle N \rangle^2] / [M - \langle N \rangle] \\ = [g\rho V + (g\rho V)^2] / [\rho V(1 - g)] = g(1 + g\rho V) / (1 - g). \quad (1)$$

The coherent and incoherent contributions to the HRS from a domain can be distinguished since the  $\langle N \rangle$  cooperative slowly relaxing molecules give a narrow peak in the HRS spectrum, while the other  $M - \langle N \rangle$  random rapidly reorienting molecules give a much broader peak. However, the single value for  $R$  that can be measured for a pure liquid with density  $\rho$  is insufficient to solve Eq. (1) for both  $g$  and  $V$ .

In the case of a binary molecular solution where HRS from one of the components is negligible,  $\rho$  in Eq. (1) may be taken as the molecular density of the strong scattering component. Then measurements of  $R(\rho)$  for several solutions with different probe concentrations  $\rho$  may provide enough information to determine the domain order parameter  $g$  and volume  $V$ . In the ideal case where  $g$  and  $V$  are independent of  $\rho$ ,  $R(\rho)$  is a linear function of  $\rho$  whose intercept and slope at  $\rho=0$  determine  $g$  and  $V$ . To approach this ideal case the dipole coupling for both molecules in the solution should be nearly the same. Nitromethane-nitrobenzene solutions were chosen with this condition in mind. This condition is not met if one of the molecules is nonpolar. The analysis becomes more complicated when the dipole coupling is a function of the composition of the solution which must also be determined from the data.

The mean orientation  $\langle \cos \theta \rangle$  for molecules with dipole moment  $\mu$  oriented by an electric field  $E$  is given by the Langevin function<sup>15</sup>

$$L(\xi) = \coth \xi - 1/\xi, \quad (2)$$

where  $\xi = \mu E / k_B T$ . Assuming the Lorentz local field  $E = P/3\epsilon_0$  for a medium with uniform polarization  $P$ , the dipole order parameter  $\langle \cos \theta \rangle$  for the molecules in a ferroelectric domain with homogenous polarization due to the dipole interaction is given by the solution of

$$p = L(3ap), \quad (3)$$

where

$$p = P/\rho\mu = \langle \cos \theta \rangle \quad (4)$$

is the fraction of saturation polarization, and

$$a = \rho\mu^2/9\epsilon_0 k_B T \quad (5)$$

is the dipole coupling parameter. The threshold dipole coupling parameter for spontaneous polarization of the medium is  $a=1$ . As shown in Fig. 1, the polarization increases very rapidly for  $a$  just above threshold, but approaches the final saturation value  $p=1$  more slowly.

For ferroelectric domains with inhomogenous polarization it is assumed that the spatial variation of the polarization is slow enough that locally it appears nearly uniform, so that the saturation parameter for the local orientational order is still  $p=p(a)$  from Eq. (3). Then the dipole order parameter for a domain is  $g=g_0p$ , where  $g_0 = \langle \cos \theta \rangle_{\max}$  is the average

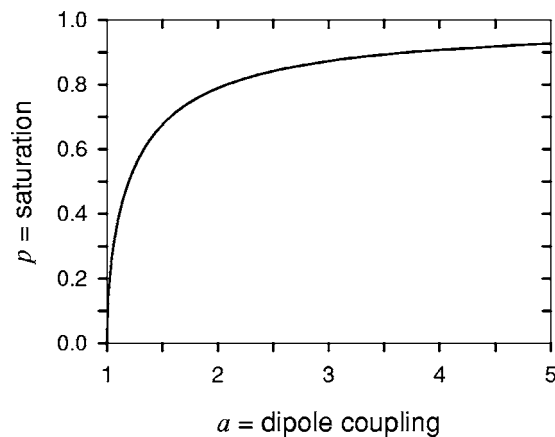


FIG. 1. Polarization saturation  $p$  as a function of the dipole coupling parameter  $a$ , calculated from Eqs. (2)–(5).

over the domain spatial distribution in the limit of a fully ordered domain ( $p=1$ ). Domains with a polarization vortex structure<sup>10,11</sup> will have  $g_0 \ll 1$ .

### III. EXPERIMENT

The apparatus is the same as previously described.<sup>2,3,5</sup> The beam from an injection seeded, single longitudinal mode, pulsed Nd:YAG (yttrium aluminum garnet) laser at  $\lambda=1064$  nm was focused into the liquid sample contained in a 1 cm fused silica fluorimeter cuvette placed in a thermostatic enclosure at  $T=27.0$  °C, and the scattered light near  $\theta=90^\circ$  and  $\lambda=532$  nm was collected with a  $f/1.8$  lens, and analyzed by a grating spectrometer with calibrated spectral response. A fiber-coupled confocal Fabry-Pérot interferometer with 1.0 GHz free spectral range (FSR) was added in series with the grating spectrometer for high-resolution measurements. The incident beam in the sample had a waist diameter of 6  $\mu\text{m}$ , and the pulses had a 2.2 kHz repetition rate, 90 ns duration, and 0.5 mJ energy. Strong focusing ( $f/5$ ) of the laser beam reduces thermal lensing effects, allows better coupling to the Fabry-Pérot, and prevents damage at the cell windows, but increases the peak intensity at the focus to 40  $\text{GW}/\text{cm}^2$ . The sample solutions of nitrobenzene (electronic grade, Acros) and nitromethane (spectrophotometric grade, Aldrich) were filtered through a 0.2  $\mu\text{m}$  micropore filter to remove dust. The polarization of the incident laser beam was controlled using a prism polarizer and an electronically controlled liquid crystal wave plate, while the polarization of the collected light was analyzed using a sheet polarizer mounted to allow the polarization axis to be rotated rapidly by  $90^\circ$ . A liquid crystal  $45^\circ$  rotator placed between the analyzing polarizer and the grating spectrometer equalized the response for  $H$  and  $V$  polarizations. The measured deviations from constant response were less than 5% for both polarizations over the  $100\text{ cm}^{-1}$  spectral range used in this work.

High-resolution HRS spectra were obtained by scanning the Fabry-Pérot over a 380 MHz range, with the grating spectrometer serving as a  $1.6\text{ cm}^{-1}$  bandwidth [full width at half maximum intensity (FWHM)] prefilter centered at the second-harmonic frequency. The HRS spectrum and the ref-

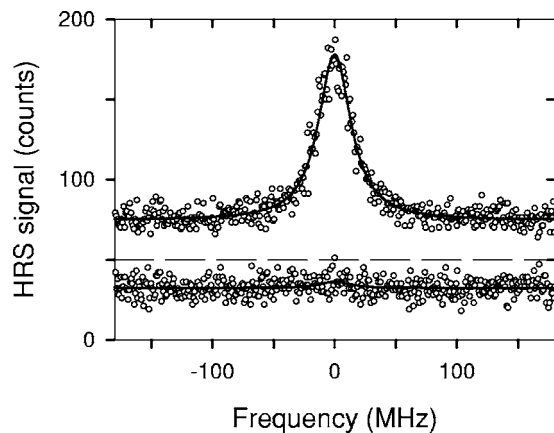


FIG. 2. Fabry-Pérot scans of the  $HV$  and  $VH$  HRS spectra for a solution of 50% nitrobenzene and 50% nitromethane by volume at 27.0 °C. The curves fitted to the data points are the sum of the scaled instrument spectral response function and a constant background. For clarity the  $VH$  data points and curve are shifted up 50 counts (base line shown dashed). The instrument spectral resolution is 35 MHz FWHM and the gated dark count is 0.08 counts/point.

erence spectrum of second-harmonic light generated in a potassium titanyl phosphate (KTP) crystal were recorded on alternate scans of the interferometer. The spectral resolution was typically 35 MHz FWHM, with the narrow peak riding on a flat background due to the 48 overlapping spectral orders for the light in the  $1.6\text{ cm}^{-1}$  band transmitted by the grating spectrometer. The HRS peak and flat background were typically 0.4 and 0.1 counts/s, respectively, and the gated photomultiplier dark count rate was  $1 \times 10^{-3}$  counts/s.

Low resolution HRS spectra were obtained using the grating spectrometer to scan a  $10\text{ cm}^{-1}$  range with  $0.4\text{ cm}^{-1}$  FWHM spectral slit width (SSW) and a  $100\text{ cm}^{-1}$  range with  $1.6\text{ cm}^{-1}$  SSW. The intensity ratios for  $VV$ ,  $HV$ , and  $VH$  HRS were also measured for a  $1.6\text{ cm}^{-1}$  wide band centered at zero frequency shift. The measurements were corrected for the instrument response, detector background, and the polarization mixing due to the finite laser focusing and light collection angle, and adjusted for detailed balance.<sup>2,5,6</sup> The low-resolution HRS signal was as large as 1000 counts/s.

TABLE I. Ratios of integrated intensities for the narrow spike and flat background in the  $VH$  HRS spectrum as a function of nitrobenzene volume fraction  $x$  in nitrobenzene-nitromethane solutions at 27.0 °C.

$x$ (%)	$R_1$	$R_2$	$R$
0 <sup>a</sup>	$0.91 \pm 0.06$	...	$0.66 \pm 0.06$
5	$0.1201 \pm 0.0046$	$0.0864 \pm 0.0046$	$0.0669 \pm 0.0036$
10	$0.1159 \pm 0.0046$	$0.0999 \pm 0.0046$	$0.0781 \pm 0.0036$
20	$0.1413 \pm 0.0064$	$0.1343 \pm 0.0064$	$0.1069 \pm 0.0051$
30	$0.1606 \pm 0.0046$	$0.1566 \pm 0.0046$	$0.1269 \pm 0.0037$
40	$0.1744 \pm 0.0046$	$0.1719 \pm 0.0046$	$0.1419 \pm 0.0038$
50	$0.1840 \pm 0.0046$	$0.1824 \pm 0.0046$	$0.1535 \pm 0.0039$
60	$0.1902 \pm 0.0046$	$0.1891 \pm 0.0046$	$0.1623 \pm 0.0039$
70	$0.1659 \pm 0.0046$	$0.1653 \pm 0.0046$	$0.1447 \pm 0.0040$
80	$0.1170 \pm 0.0046$	$0.1166 \pm 0.0046$	$0.1041 \pm 0.0041$
90	$0.0937 \pm 0.0037$	$0.0935 \pm 0.0037$	$0.0852 \pm 0.0034$
95	$0.0639 \pm 0.0046$	$0.0638 \pm 0.0046$	$0.0588 \pm 0.0042$
100	$0.0455 \pm 0.0046$	$0.0455 \pm 0.0046$	$0.0424 \pm 0.0043$

<sup>a</sup>Reference 5.

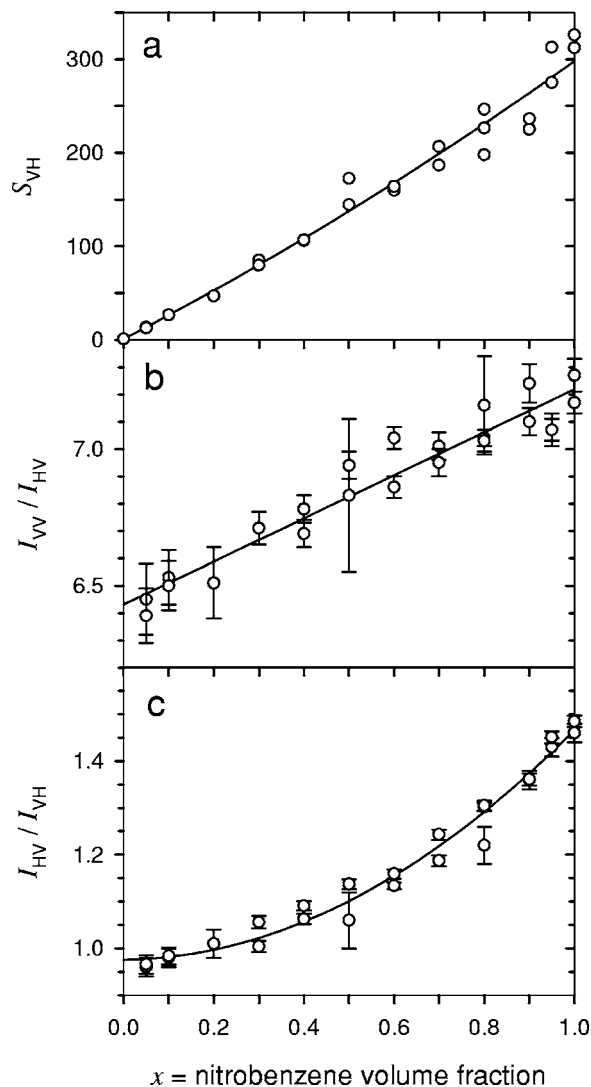


FIG. 3. HRS intensity and polarization ratios for nitrobenzene-nitromethane solutions at 27.0 °C measured with a  $1.6\text{ cm}^{-1}$  spectral window centered at zero frequency shift. Error bars shown for the data points only include counting statistics. (a) Solution  $VH$  HRS intensity  $S_{VH}$ , normalized to nitromethane  $VH$  HRS intensity, vs nitrobenzene volume fraction  $x$ . Fitted curve is  $S_{VH} = 1 + 250.2x + 46.5x^2$ . (b) Polarization ratio  $I_{VV}/I_{HV}$  vs  $x$ . Fitted curve is  $I_{VV}/I_{HV} = 6.431 + 0.788x$ . (c) Polarization ratio  $I_{HV}/I_{VH}$  vs  $x$ . Fitted curve is  $I_{HV}/I_{VH} = 0.9755 + 0.0108x + 0.4797x^2$ .

#### IV. RESULTS AND ANALYSIS

Figure 2 shows an example of the high-resolution HRS spectra obtained using the Fabry-Pérot interferometer. The peak in the  $VH$  HRS spectrum is instrumentally broadened and the spectrum is adequately fit with a curve which is the sum of the scaled instrument spectral response function and a constant background. The true width of the peak in the HRS spectrum is estimated by fitting a function which is the convolution of the instrument spectral function with a Lorentzian representing the true HRS spectrum. The Lorentzian for the best fit has zero width, and the upper bound on the Lorentzian bandwidth is 4 MHz FWHM at the 99% confidence level, corresponding to a relaxation time  $\tau > 80$  ns. The narrow peak in the  $VH$  HRS spectrum is absent from the  $HV$  and  $VV$  spectra. The very weak peak seen in the  $HV$  HRS spectrum shown in Fig. 2 is accounted for by leakage of  $VH$

TABLE II. HRS spectral fit parameters for Eq. (8) for solutions with volume fraction  $x$  of nitrobenzene in nitromethane at  $T=27.0$  °C. These parameters are obtained from simultaneous fits to 100  $\text{cm}^{-1}$  spectral scans with 1.6  $\text{cm}^{-1}$  SSW and 10  $\text{cm}^{-1}$  scans with 0.4  $\text{cm}^{-1}$  SSW. The HRS intensity is dominated by scattering from nitrobenzene, except at  $x=0$  where it is entirely due to nitromethane, so the  $x=0$  points do not follow the trend for the other points.

$x$	0.0 <sup>a</sup>	0.2	0.4	0.6	0.8	1.0
$\nu_1$ ( $\text{cm}^{-1}$ )	1.28	0.368	0.306	0.255	0.201	0.157
$\nu_2$ ( $\text{cm}^{-1}$ )	6.63	1.79	1.78	1.63	1.32	1.12
$\nu_3$ ( $\text{cm}^{-1}$ )	50.6	20.4	19.7	19.3	19.2	18.7
$A_{VV}/A_{HV}$	7.71	8.86	8.44	8.56	8.50	9.00
$B_{VV}/B_{HV}$ <sup>b</sup>	1.79	2.10	2.15	2.10	2.30	2.32
$A_{HV}/B_{HV}$	1.82	4.16	6.27	8.29	9.16	11.52
$B_{HV}/C_{HV}$	2.93	14.3	13.2	12.8	16.7	17.9

<sup>a</sup>Reference 5.

<sup>b</sup> $C_{VV}/C_{HV}=B_{VV}/B_{HV}$ .

light into the  $HV$  spectrum due to the large collection angle.<sup>6</sup> The observed  $HV$  peak is  $4\% \pm 1.5\%$  of the  $VH$  peak intensity, in good agreement with the 5% predicted intensity due to leakage.

The ratio of coherent and incoherent HRS intensities  $R$  defined in Eq. (1) is experimentally determined from high-resolution  $VH$  HRS spectra such as that shown in Fig. 2. The coherent intensity is obtained from the integrated intensity of the peak. The incoherent intensity is obtained from the intensity of the flat background integrated over the 1.0 GHz FSR of the Fabry-Pérot spectrometer, which includes all the light within the 1.6  $\text{cm}^{-1}$  spectral window selected by the grating spectrometer due to overlap of successive orders of the Fabry-Pérot interferometer. The ratio  $S/B$  of the spike ( $S$ ) and background ( $B$ ) integrated intensities is given for several nitrobenzene concentrations in the second column of Table I labeled  $R_1$ . This ratio differs from the desired ratio  $R$  in two ways. First, it includes the HRS contribution from nitromethane as well as that from nitrobenzene. The nitromethane contribution is small, but it can be significant since the spike-to-background ratio for nitromethane is much larger than for nitrobenzene. Second, part of the rotational HRS spectrum may fall outside the 1.6  $\text{cm}^{-1}$  spectral window and not have been included. Additional information from low-resolution HRS measurements is used to extract  $R$  from  $R_1$ .

The first correction makes use of HRS intensities measured with a 1.6  $\text{cm}^{-1}$  spectral window centered at zero frequency shift. Figure 3 shows  $S_{VH}$ , the solution  $VH$  intensities normalized to the  $VH$  intensity for neat nitromethane, versus nitrobenzene volume fraction  $x$ . The  $VH$  HRS intensity for neat nitrobenzene is  $300\times$  larger than that for neat nitromethane (the  $HV$  intensity is  $750\times$  larger). Also shown in Fig. 3 are the measured polarization ratios  $I_{VV}/I_{HV}$  and  $I_{HV}/I_{VH}$  vs  $x$ . The ratio  $R_2$  obtained by removing the nitromethane contribution from  $R_1$  is given by

$$R_2 = \frac{R_1 - R_{1,NM}Q}{1 - Q}, \quad (6)$$

$$Q = \frac{1 + R_1}{1 + R_{1,NM}} \frac{1 - x}{S_{VH}}, \quad (7)$$

where  $R_{1,NM}$  is  $R_1$  for neat nitromethane (NM). This correction reduces  $R_2$  by 30% for the most dilute solution, as shown in Table I.

The second correction accounting for the wings of the reorientation spectrum uses the low-resolution  $VV$  and  $HV$  spectra, which are decomposed into several overlapping components of different width and polarization dependence. The analysis does not use the low-resolution  $VH$  spectrum directly since components narrower than the resolution of the grating spectrometer account for both the narrow and wide components in the  $VH$  Fabry-Pérot spectrum, and this makes dissection of these components unreliable using just the low-resolution  $VH$  spectrum. The spectra are fit with a function of the form,

$$I(\nu) = A[1 + (\nu/\nu_1)^2]^{-1} + B[1 + (\nu/\nu_2)^2]^{-1} + C \exp[-|\nu/\nu_3|] + D\delta(\nu), \quad (8)$$

convolved with the instrument spectral response function.<sup>5</sup> The first term in Eq. (8) is due to the fast molecular reorientation which gives the flat background in the Fabry-Pérot spectrum, the next two terms represent the broad spectrum induced by intermolecular collisions, and the last term is the narrow spike due to slowly relaxing domains. The frequencies  $\nu_1$ ,  $\nu_2$ , and  $\nu_3$  are independent of polarization, but the coefficients  $A$ ,  $B$ ,  $C$ , and  $D$  are not. For the  $VV$  and  $HV$  spectra,  $D=0$ . The results of these fits are given in Table II. The width parameters from the fit allow one to evaluate for each component the fraction  $t$  of the integrated intensity falling within the 1.6  $\text{cm}^{-1}$  spectral window, e.g.,  $t_A = (2/\pi)\arctan(1.6\text{cm}^{-1}/2\nu_1)$ .

The HRS intensity within the 1.6  $\text{cm}^{-1}$  spectral window can be partitioned according to polarization dependence into four terms,  $F_1$ ,  $F_2$ ,  $F_3$ , and  $F_4$ , where  $I_{HV}=F_1+F_2+F_4$  and  $I_{VH}=F_1+1/2F_2+F_3+F_4$ . The combined terms  $F_1$  and  $F_2$  correspond to the  $A$  term in Eq. (8),  $F_3$  corresponds to the  $D$  term, and  $F_4$  corresponds to the combined  $B$  and  $C$  terms. The  $F_1$  and  $F_2$  terms are due to isotropic local and transverse polar collective orientation modes, respectively. The spectral distribution appears to be the same for these two modes but



TABLE III. Fit parameters for  $R(x)$  vs  $x$  for the data in Table I and the function given by Eqs. (12) and (13).

Parameter	Value
$g_0$	$0.053 \pm 0.005$
$V$	$20.3 \pm 5.6 \text{ nm}^3$
$a_0$	$0.053 \pm 0.014$
$a_1$	$0.47 \pm 0.19$
$a_2$	$2.98 \pm 1.79$

the polarization dependence is different. The desired ratio of  $VH$  spectral intensities  $R = t_A F_3 / (F_1 + 1/2 F_2)$  is determined by combining the  $VV$ ,  $HV$ , and  $VH$  experimental measurements as follows:

$$R = t_A R_2 (1 + R_4 / R_3), \quad (9)$$

$$R_3 = \frac{(1 + R_4)}{(1 + R_2)(I_{HV}/I_{VH})} - R_4, \quad (10)$$

$$R_4 = F_4 / (F_1 + F_2), \quad (11)$$

where  $I_{HV}/I_{VH}$  is given in Fig. 3 and  $R_4$  is evaluated from the spectral fit parameters in Table II. The factor  $t_A$  accounts for the wings of the reorientation spectrum which fall outside the  $1.6 \text{ cm}^{-1}$  window, and the  $R_4/R_3$  term in Eq. (9) subtracts the contribution from the collision-induced spectrum. The factor  $R_3 = (F_1 + 1/2 F_2) / (F_1 + F_2)$  differs from 1 due to the nonzero transverse mode contribution  $F_2$ . The transverse mode fraction  $F_2 / (F_1 + F_2) = 2(1 - R_3)$  increases from 0.23 at  $x=0.2$  to 0.71 at  $x=1$  (fit =  $1.26x - 0.55x^2$ ). The final results for  $R$  are given in the last column of Table I. The intensity ratio  $R$  is 20% lower than  $R_2$  for the most dilute solution.

The final step in the analysis is to fit the  $R(x)$  data with the function

$$R(x) = g_0 p (1 + g_0 p x \rho_{\text{NB}} V) / (1 - g_0 p), \quad (12)$$

where  $\rho_{\text{NB}} = 9.8 \text{ M} = 5.90 \text{ nm}^{-3}$  is the molecular number density for neat nitrobenzene,  $x$  is the nitrobenzene volume fraction,  $V$  is the domain volume,  $p = p(a) = L(3ap)$  is the polarization saturation function shown in Fig. 1, and

$$a(x) = 1 + a_0 + a_1(1 - x) + a_2(1 - x)^2 \quad (13)$$

is the concentration-dependent dipole coupling parameter. The fit parameters are  $g_0$ ,  $V$ ,  $a_0$ ,  $a_1$ , and  $a_2$ , and the results are given in Table III and shown in Fig. 4.

## V. DISCUSSION

The dipole order parameter  $g_0 = 0.053$  obtained from the fit shown in Fig. 4 is consistent with the polarization vortex structure seen in calculations for the Stockmayer model dipolar fluid, and the domain volume  $V = 20.3 \text{ nm}^3$  obtained from the fit is only slightly smaller than the cell size used in those calculations.<sup>10,11</sup> This fit gives the order parameter and size for domains in pure nitromethane, assuming that  $g_0$  and  $V$  are independent of the nitrobenzene probe molecule concentration. The results for  $g_0$  and  $V$  should be reliable even if this assumption is not strictly true, since they are obtained

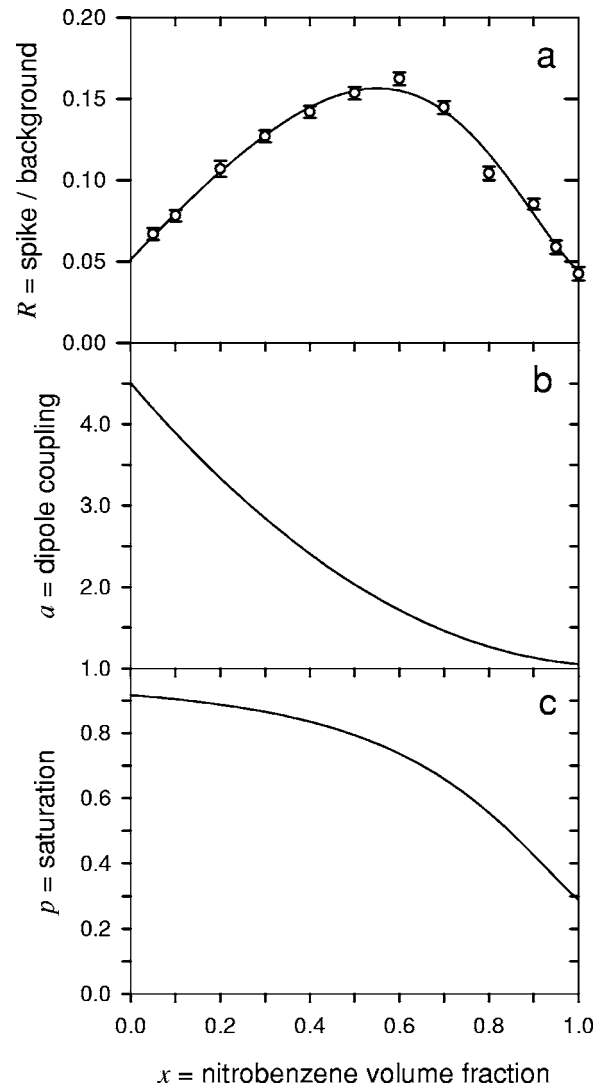


FIG. 4. Fit to the data for the spike-to-background intensity ratio  $R(x)$  obtained from Fabry-Pérot  $VH$  HRS spectra. (a) Data points (open circles) for  $R$  are from Table II and fitted curve is Eqs. (12) and (13) with parameters from Table III. The zero intercept gives the domain dipole order parameter  $g_0$ , and the initial slope gives the domain volume  $V$ . (b) Dipole coupling function  $a(x)$  obtained from the fit. (c) Local polarization saturation function  $p(x)$  obtained from the fit.

essentially from the zero intercept and initial slope of the fitted curve which are determined mainly by the lowest concentration points. The domain volume  $V$  determined from the fit contains 229 nitromethane molecules ( $\rho = 18.7 \text{ M}$ ) or 120 nitrobenzene molecules ( $\rho = 9.8 \text{ M}$ ), and corresponds to a sphere with 3.4 nm diameter.

The dipole coupling is a free parameter for the fit in Fig. 4. The value returned by the fit in the limit of pure nitromethane is  $a(0) = 4.51$ , consistent with  $a = 4.57$  calculated using the gas phase dipole moment  $\mu_0 = 3.46 \text{ D}$  for nitromethane in Eq. (5). The saturation parameter at  $x=0$  is  $p = 0.91$ , indicating a high degree of orientational order for the molecules in a domain in neat nitromethane. These results are consistent with two other independent measurements. For pure nitromethane, the HRS signal is entirely due to the nitromethane molecules and one can predict  $R$  using an expression analogous to Eq. (12),

$$R_{\text{NM}} = g_0 p (1 + g_0 p \rho_{\text{NM}} V) / (1 - g_0 p). \quad (14)$$

Evaluating Eq. (14) using the values  $g_0=0.053$ ,  $p=0.91$ , and  $\rho_{\text{NM}}V=229$  obtained from the fit in Fig. 4 gives  $R_{\text{NM}}=0.62$ , in good agreement with the direct experimental measurement  $0.66\pm 0.06$  for neat nitromethane reported in Table I.<sup>5</sup> A second consistency check comes from hyperpolarizability measurements. The strong local order of the molecules indicated by  $p=0.91$  for neat nitromethane will result in a polarization field  $E=p\rho_{\text{NM}}\mu_0/3\epsilon_0=4.4$  GV/m oriented parallel to the molecular dipole moment. The first hyperpolarizability  $\beta(E)$  for molecules in the presence of this electric field in the liquid will be  $\beta(E)=\beta_{\parallel}+\gamma E$ , where  $\beta_{\parallel}=-1.08\times 10^{-51}$  C<sup>3</sup> m<sup>3</sup> J<sup>-2</sup> and  $\gamma=2.93\times 10^{-61}$  C<sup>4</sup> m<sup>4</sup> J<sup>-3</sup> are the first and second hyperpolarizabilities for nitromethane measured in the gas phase.<sup>16</sup> The increment  $\gamma E$  is larger than  $\beta_{\parallel}$  and of the opposite sign, so that  $\beta(E)/\beta_{\parallel}=-0.19$  is predicted for liquid nitromethane. The ratio of liquid and gas phase hyperpolarizabilities  $|\beta_L/\beta_G|=0.52\pm 0.05$  was previously estimated from a measurement of the VV HRS integrated intensity ratio for liquid and gas phase nitromethane.<sup>16</sup> However, the “allowed” spectrum due to molecular reorientation accounts for only 36% of the VV HRS integrated intensity in the liquid, and the collision-induced spectrum due to rapid random fluctuations in  $\beta$  during short range intermolecular interactions accounts for the rest.<sup>5</sup> A better estimate is  $|\beta_L/\beta_G|=0.52(0.36)^{1/2}=0.31$  based on the ratio of intensities for just the reorientation spectra, in fair agreement with the estimate  $\beta(E)/\beta_{\parallel}=-0.19$  that follows from the measured ferroelectric domain parameters.

The dipole coupling parameter for neat nitrobenzene from the fit in Fig. 4 is  $a(1)=1.05$ , much smaller than  $a=3.57$  calculated using Eq. (5) with the gas phase dipole moment  $\mu_0=4.22$  D for nitrobenzene. Even with this near-threshold value for the coupling, the saturation parameter  $p=0.29$  is not small. A lowered value for the dipole coupling parameter can occur by the formation of antiparallel centrosymmetric pairs of nitrobenzene molecules having zero dipole moment and first hyperpolarizability. Evidence for just such nearest neighbor correlations comes from a recent molecular dynamics simulation of liquid nitrobenzene which finds a strong tendency for close face-to-face packing of the phenyl rings with antiparallel alignment of the dipole moments.<sup>17</sup> The dipole interaction favors parallel orientation for a dipole placed on the polar axis of another dipole and antiparallel orientation for equatorial dipoles, with zero net orientation for randomly distributed nearest neighbor dipoles. It appears that the long range dipole coupling is reduced almost to threshold in nitrobenzene as a result of the preferred equatorial packing of nearest neighbor molecules.

The transverse polar, longitudinal polar, and isotropic mode contributions to the HRS spectra are distinguished by their polarization dependence:  $I_{HV}/I_{VH}=2$ , 0, or 1, respectively. For neat nitrobenzene the present work gives  $I_{HV}/I_{VH}=1.47\pm 0.01$  (measured with  $1.6$  cm<sup>-1</sup> SSW, see Fig. 3), as compared to previous results  $1.44\pm 0.10$  ( $4.2$  cm<sup>-1</sup> SSW),<sup>18</sup> and  $1.08\pm 0.01$  ( $25$  cm<sup>-1</sup> SSW).<sup>19</sup> The present result indicates a large transverse polar collective mode contribution to the reorientation spectrum, and the transverse mode

intensity fraction estimated for neat nitrobenzene is  $F_2/(F_1+F_2)=0.71$  [see Eq. (10) and following]. Also measured in this work is the polarization ratio  $I_{VV}/I_{HV}=7.2\pm 0.1$  ( $1.6$  cm<sup>-1</sup> SSW, see Fig. 3), as compared to previous results  $I_{VV}/I_{HV}=7.6\pm 0.2$  ( $25$  cm<sup>-1</sup> SSW),<sup>19</sup> and  $I_{VV}/I_{VH}=8.7$  ( $4.2$  cm<sup>-1</sup> SSW) (Ref. 18) from which one obtains  $I_{VV}/I_{HV}=8.7/1.44=6.0$ . The estimated transverse mode contribution given above is consistent with  $I_{VV}/I_{HV}$  observed in the present work. Identifying the transverse mode contribution as the narrow reorientation peak ( $\nu_1=0.157$  cm<sup>-1</sup>) in the VV and HV spectra with  $A_{VV}/A_{HV}=9.0$ , the isotropic mode contribution as the collision-induced spectrum with  $B_{VV}/B_{HV}=2.3$  (see Table II), and assuming intensity fractions 0.71 and 0.29 for the transverse and isotropic mode contributions, one estimates  $I_{VV}/I_{HV}=7.1$ , in good agreement with  $I_{VV}/I_{HV}=7.2\pm 0.1$  from direct measurement. This agreement, and the fact that  $A_{VV}/A_{HV}=9.0$  is exactly the polarization ratio expected for a transverse mode, both suggest that the narrow reorientation peak in the VV and HV HRS spectra for neat nitrobenzene is a pure transverse mode.

As the nitrobenzene concentration decreases the ratio  $I_{HV}/I_{VH}$  also decreases (Fig. 3 and Ref. 18). This is due to a strongly decreasing transverse mode contribution and a weakly increasing longitudinal mode contribution. The ratio  $I_{VV}/I_{HV}$  also decreases, but the polarization ratios  $A_{VV}/A_{HV}$  and  $B_{VV}/B_{HV}$  for the reorientation and collision-induced spectra are nearly independent of nitrobenzene concentration. The narrow reorientation peak must become a mixed transverse and isotropic mode to reconcile the observed values of  $I_{VV}/I_{HV}$  with the estimated transverse mode contributions  $F_2/(F_1+F_2)$ . The transverse mode fraction for the reorientation peak decreases to 0.37 for the 20% nitrobenzene solution.

The main results of this work are the measurements of the size and order parameter for the ferroelectric domains in liquid nitromethane. The domains have a volume of  $20$  nm<sup>3</sup> containing 230 nitromethane molecules and relax on a time scale  $>80$  ns. The observations are consistent with orientational order in the form of a polarization vortex with maximal dipole order parameter  $g_0=0.053$ . For nitromethane the measured order parameter is 91% of the saturated value. For liquid nitrobenzene, short range antiparallel orientational correlations between the molecules reduce the dipole coupling to near the ferroelectric threshold, and the measured order parameter is only 29% of the saturated value.

<sup>1</sup>D. P. Shelton, Phys. Rev. B **72**, 020201(R) (2005).

<sup>2</sup>D. P. Shelton, J. Chem. Phys. **117**, 9374 (2002); **121**, 3349(E) (2004).

<sup>3</sup>D. P. Shelton, J. Chem. Phys. **123**, 084502 (2005).

<sup>4</sup>D. P. Shelton and P. Kaatz, Phys. Rev. Lett. **84**, 1224 (2000).

<sup>5</sup>D. P. Shelton, J. Chem. Phys. **123**, 111103 (2005).

<sup>6</sup>D. P. Shelton, J. Opt. Soc. Am. B **17**, 2032 (2000).

<sup>7</sup>V. N. Denisov, B. N. Mavrin, and V. B. Podobedov, Phys. Rep. **151**, 1 (1987).

<sup>8</sup>V. N. Denisov, B. N. Mavrin, V. B. Podobedov, and Kh. E. Sterin, Opt. Commun. **44**, 39 (1982).

<sup>9</sup>B. Groh and S. Dietrich, Phys. Rev. E **55**, 2892 (1997).

<sup>10</sup>B. Groh and S. Dietrich, Phys. Rev. E **57**, 4535 (1998).

<sup>11</sup>B. Groh and S. Dietrich, Phys. Rev. Lett. **79**, 749 (1997).

<sup>12</sup>I. I. Naumov, L. Belaiche, and H. Fu, Nature (London) **432**, 737 (2004).

- <sup>13</sup>H. Fu and L. Bellaiche, Phys. Rev. Lett. **91**, 257601 (2003).
- <sup>14</sup>S. T. Lagerwall, J. Phys.: Condens. Matter **8**, 9143 (1996).
- <sup>15</sup>C. Kittel, *Introduction to Solid State Physics*, 4th ed. (Wiley, New York, 1971).
- <sup>16</sup>P. Kaatz, E. A. Donley, and D. P. Shelton, J. Chem. Phys. **108**, 849 (1998).
- <sup>17</sup>R. H. C. Janssen, D. N. Theodorou, S. Raptis, and M. G. Papadopoulos, J. Chem. Phys. **111**, 9711 (1999).
- <sup>18</sup>J. Chen and K. Y. Wong, J. Chem. Phys. **122**, 174505 (2005).
- <sup>19</sup>D. P. Shelton, Chem. Phys. Lett. **325**, 513 (2000).